Photohalogen Elimination Chemistry in Low-valent Binuclear Nickel Complexes

Seung Jun Hwang, a,b Ryan G. Hadt, c,d Serge Ruccolo, David Gygi, Shao-Liang Zheng, Yu-Sheng Chen, and Daniel G. Nocera, David Gygi, Shao-Liang Zheng, David Gygi, Shao-Liang Zheng, Yu-Sheng Chen, and Daniel G. Nocera, Shao-Liang Zheng, Shao-Liang

^a Department of Chemistry and Chemical Biology, Harvard University, 12 Oxford Street, Cambridge, MA 02138. ^b Department of Chemistry, POSTECH, Pohang 37673, Korea. ^c Chemical Sciences and Engineering Division, Argonne National Laboratory, Lemont, IL 60439. ^d Division of Chemistry and Chemical Engineering, California Institute of Technology, Pasadena, CA 91125. ^e ChemMatCARS, The University of Chicago, Argonne, IL 60439.

Keywords: solar, photoactivation, metal-chloride, metal-metal, hydrohalic acid splitting, photocrystallography

ABSTRACT: The photogeneration of X_2 is the key to achieving an efficient HX-splitting photocycle, as it is more thermodynamically and kinetically challenging than its H_2 half reaction counterpart. Here we report a strategy that enables Cl_2 photoelimination from low-valent binuclear d^9 – d^9 and d^9 – d^{10} Ni complexes. We demonstrate the importance of metal–metal bond interaction for M–X bond photoactivation with a combination of TD-DFT computations together with spectroscopy and photocrystallography, exemplifying a design principle for future developments of 3d metal complexes for HX photocatalysis.

1. Introduction

The photochemical splitting of HX (X=Cl, Br) into X_2 and H_2 is an alternative strategy to storing solar energy in chemical bonds, as compared to the more common strategy afforded by water splitting. 1-3 Although HX-splitting is only a two electron and two proton processes, the design of a catalytic system that can simultaneously execute the photoelmination of X2 from M-X bonds and H₂ evolution from HX efficiently on one discrete metal complex constitutes a difficult challenge owing to the thermodynamically and kinetically demanding photoelimination step, which is the bottleneck to closing HXsplitting photochemical cycles. ⁴ Successful M-X photoactivation has primarily been relegated to 2^{nd} and 3^{rd} row mono- and bi-nuclear metal complexes, $^{5-}$ 12 and main group complexes, $^{13-}$ 18 with more limited success involving metal complexes of the 1st row. 19 - 22 Moving to the 1st row transition elements for photochemical HXsplitting platforms presents the challenge that their complexes often exhibit short excited state lifetimes because of fast, energy wasting, internal conversion processes. ^{23,24} In this regard, achieving halogen photoelimination with 1st row transition metal complexes requires specific ligand design to direct the nonradiative decay along a to M-X photocleavage pathway. High-yielding endothermic Cl2 photoelimination chemistry from mononuclear Ni(III) complexes has been achieved utilizing a strategy based on secondary coordination sphere effects to suppress the undesired rapid recombination reaction. 20,21 Nonetheless, the requisite two-electron chemistry of HX splitting, common to two-electron reductive elimination observed for Ni-catalyzed cross-coupling reactions, 25-30 is hampered by one-electron photoreactions from mononuclear Ni(III) complexes and the extremely short charge-separated excited lifetime of the 1st row transition metal complex. ^{31, 32} Accordingly, photochemically generated mono- and binuclear Ni(I) halide

complexes^{19, 33, 34} were not effective for promoting photohalogen elimination chemistry.

In order to overcome the challenges confronting metal-halide bond activation from Ni complexes, we targeted a design strategy in which the photochemistry is driven by utilizing the electronic structure of the three-fold symmetry metal-metal bonding interactions as illustrated in the qualitative molecular orbital diagrams of Figure 1. Owing to the ligand field of interacting trigonal bipyramidal and octahedral metal centers, a single metal-metal bond is conserved across the d^9-d^9 , d^7-d^9 , d^7-d^7 series with $d\sigma$ and $d\sigma^*$ molecular frontier orbitals arising from the dz2 orbital interaction of neighboring d^7/d^9 metal centers. We expand on the d^7-d^7 , d^9-d^7 , and d9-d9 homo- and heterobimetallic dirhodium and diplatinum complexes, which possess both M-M and M-X antibonding character, such that electronic excitation into the empty do* orbital weakens the M-M and M-X framework, thereby promoting halogen elimination.^{3,6,35-37} Herein, we report low-valent bimetallic Ni complexes that support efficient photochemical X2 elimination.

2. Results and discussion

Comproportionation of $Ni(cod)_2$ and $NiCl_2(PPh_3)_2$, (cod = 1,5-cyclooctadiene) with 3 equivalents of the phosphazane tfepma ligand (tfepma = $((CF_3CH_2O)_2P)_2NCH_3$) yields the diamagnetic $Ni_2[I_1I]$ (tfepma) $_3Cl_2$ complex 1. Bromide complex 2 was also prepared in an analogous way with $NiBr_2(PPh_3)_2$. Treatment of 1 or 2 with 2 equivalents of CN^tBu in THF affords the one-electron reduced paramagnetic $Ni_2[I_1O]$ (tfepma) $_3(CN^tBu)(X)$ complexes 3 (X = Cl) and 4 (X = Br).

These paramagnetic complexes display no resonances in the ${}^{1}H$ NMR and ${}^{1}H$ } ${}^{31}P$ NMR spectrum. EPR spectroscopy (Figure 2) indicates complexes **3** and **4** are $S = \frac{1}{2}$, as expected for a binuclear $d^{9}-d^{10}$ complex with additional hyperfine couplings to phosphorus

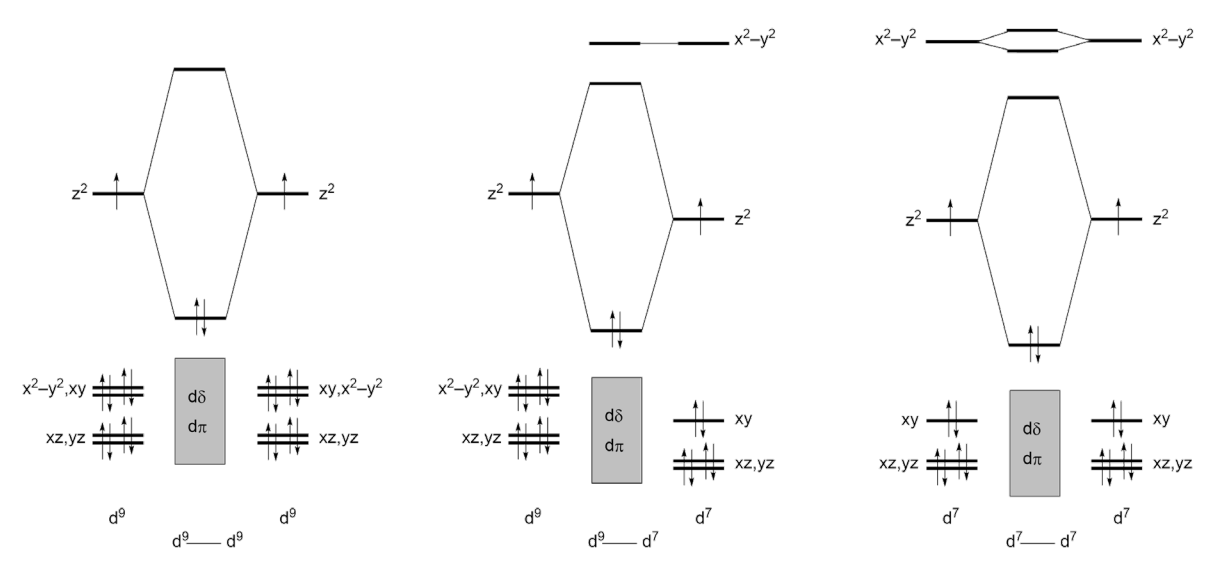


Figure 1. Qualitative molecular orbital level diagram for the interaction of d^7 (pseudo octahedral) and d^9 (pseudo trigonal bipyramidal) fragments. The dp and dd symmetry orbitals are filled and indicated by the shaded box. To minimize level congestion, the $d\sigma$ -dσ* splitting is isolated from that of the $d\pi$ and $d\delta$ orbital manifold.

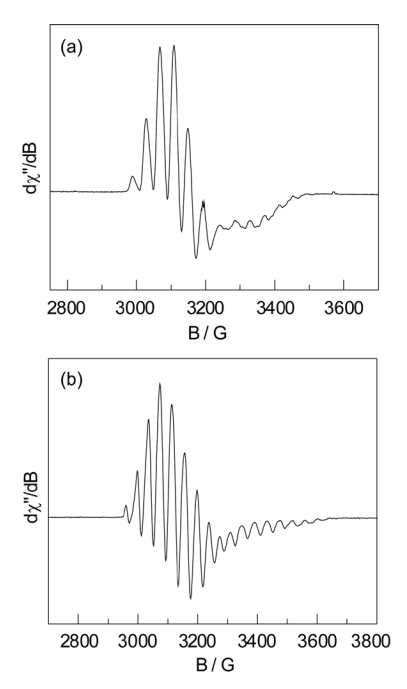


Figure 2. EPR spectra of $Ni_2[I,0]$ complexes (a) 3 and (b) 4 recorded at 77.0 K in 2-MeTHF glass.

and halide atoms, demonstrating that the unpaired electron occupies the do* orbital. As shown in Figure S18, the IR spectra of complexes **3** and **4** show a $\nu_{\rm CN} = 2152$ and 2145 cm⁻¹ respectively, consistent with a terminally bound isocyanide ligand. Treatment of **3** with 0.5 equivalents of iodobenzene dichloride, (PhICl₂), in C_6H_6 regenerates **1**.

The molecular structures of complexes 1 and 3 have been determined by X-ray diffraction and show three-fold symmetry with three bridging tfepma ligands and two five-coordinate nickel centers in a trigonal bipyramidal environment (Figure 3). A Ni–Ni distance of 2.5908(7) Å is observed for complex 1, indicating a formal metal—

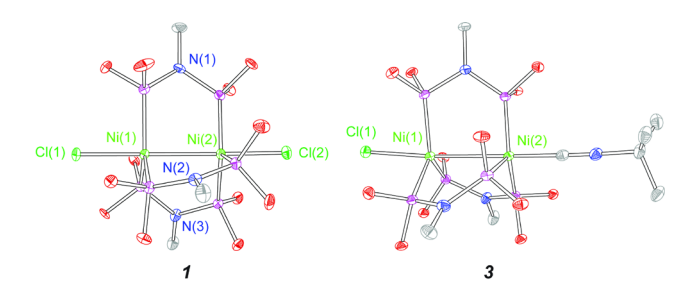


Figure 3. Thermal ellipsoid plots of **1** and **3**, drawn at 50% probability. The H atoms and $-CH_2CF_3$ groups have been removed for clarity.

metal bond that is consistent with previously reported d°-d° binuclear Ni complexes. ^{38, 39} The molecular structure of complex **3** shown in Figure 3 confirms the spectral findings of a bimetallic core that possesses two asymmetric trigonal bipyramidal Ni centers featuring isocyanide and chloride ligands. The Ni–Ni and Ni–Cl distances of 2.8686(5) and 2.4290(7) Å in complex **3** are elongated in comparison to those of complex **1**, 2.5908(7) and 2.2642(9) Å respectively, thereby confirming the population of the do* orbital, which possesses anti-bonding character with respect to Ni–Ni and Ni–Cl bonds.

Two electron reduced $Ni_2[0,0]$ (tfepma) $_3$ (CN'Bu) $_2$ complex $\bf 5$ is obtained when $\bf 1$ is treated with 2 equivalents of Cp_2^*Co (Cp_2^*Co = bis(cyclopentadienyl)cobalt(II)) and 2 equivalents of CN'Bu. The isocyanide bound $Ni_2[0,0]$ (tfepma) $_3$ (CN'Bu) complex $\bf 6$ was prepared analogously from treatment of $\bf 3$ with 1 equivalent of Cp_2^*Co in THF. In the absence of isocyanide, treatment of the $Ni_2[I,I]$ complex $\bf 1$ with 1 or 2 equivalents of $CoCp_2^*$ afforded the $[Ni_2[I,0]$ (tfepma) $_3Cl_2[CoCp_2^*]$ complex $\bf 7$ and $[Ni_2[0,0]$ (tfepma) $_3Cl_2[CoCp_2^*]$, complex $\bf 8$, respectively. Complexes $\bf 5$ and $\bf 6$ feature terminal isocyanide ligand stretching frequencies (ν_{CN} = 2094 and 2150 cm $^{-1}$, respectively) in the IR spectra (Figure S19), consistent with dppm bridged dinuclear nickel complexes.

The molecular structures of both 5 and 6 have been characterized

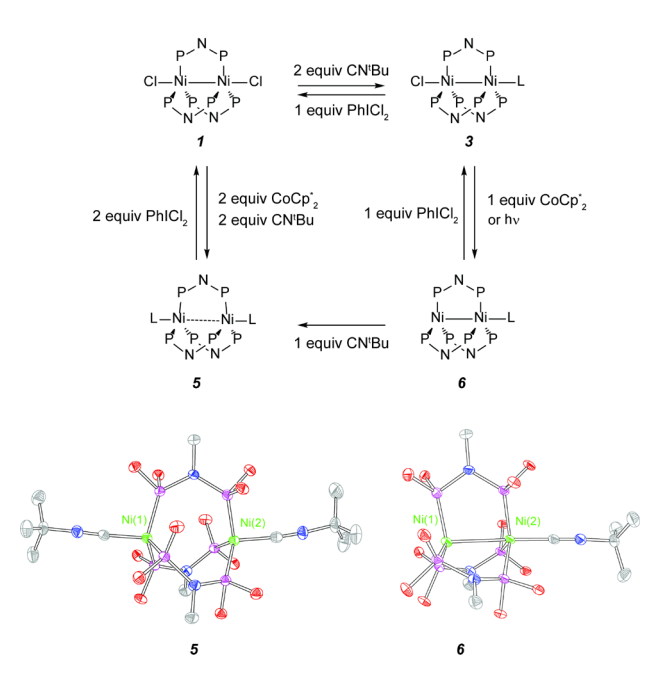


Figure 4. Synthetic relationships between tfepma bridged Ni_2 complexes. Thermal ellipsoid plots of **5** and **6**, drawn at the 50% probability level. The H atoms and $-CH_2CF_3$ are omitted for clarity.

by X-ray diffraction, and are illustrated in Figure 4. The structure of complex **5** shows two distorted tetrahedral Ni(0) centers bridged by three tfepma ligands, where the Ni–Ni distance is 3.8094(1) Å, thereby confirming the absence of a significant Ni–Ni interaction, as expected for two d¹⁰ metal centers. Interestingly, complex **6** features a coordinatively unsaturated Ni(0) center and displays a much shorter Ni–Ni distance of 2.6413(5) Å, which suggests a polarized Ni(0)/Ni(0) interaction. The formation of a dative bond from the electron rich unsaturated Ni(1) to the electron poor isocyanide-bound Ni(2), as a result of π -backbonding, could give rise to the short Ni–Ni bond distance. Treatment of **6** with 1 equivalent of CN¹Bu affords complex **5**, as confirmed by {¹H}³¹P NMR spectroscopy. Chemical oxidation of complexes **5** and **6** using PhICl² as a solid chlorine surrogate yields complexes **1** and **3**, respectively.

The absorption spectra of complexes 1 and 2 are presented in Figure S29. Both complexes exhibit distinct and intense absorption bands in the near-UV that are influenced primarily by the nature of the halide. The absorption maximum of dichloride complex 1 appears at 401 nm, whereas the maximum of the dibromide analogue 2 is red shifted to 426 nm. Calculated absorption spectra of 1 and 2 using time-dependent density functional theory (TD-DFT) are given in Figure S34 and satisfactorily reproduce the experimental trend. The TD-DFT calculated states of 1 and 2 are also given in Tables S14 and S15, respectively; the prominent absorption bands can be assigned to a combination of halide ligand-to-metal charge transfer (LMCT) and metal-to-metal charge transfer (MMCT) transitions (donor and acceptor orbitals are given in Figures S36 and S37). In contrast, d^9-d^{10} complex 3 has an absorption spectrum that exhibits a low energy band at ~650 nm and additional bands in the ~325 - 400 nm range and >300 nm (Figures 5a and S30). These absorption bands also shift to lower energy in bromide complex 4 (Figure S30). TD-DFT calculations suggest that the low energy feature is MMCT in character, whereas the absorptions in the 350 -

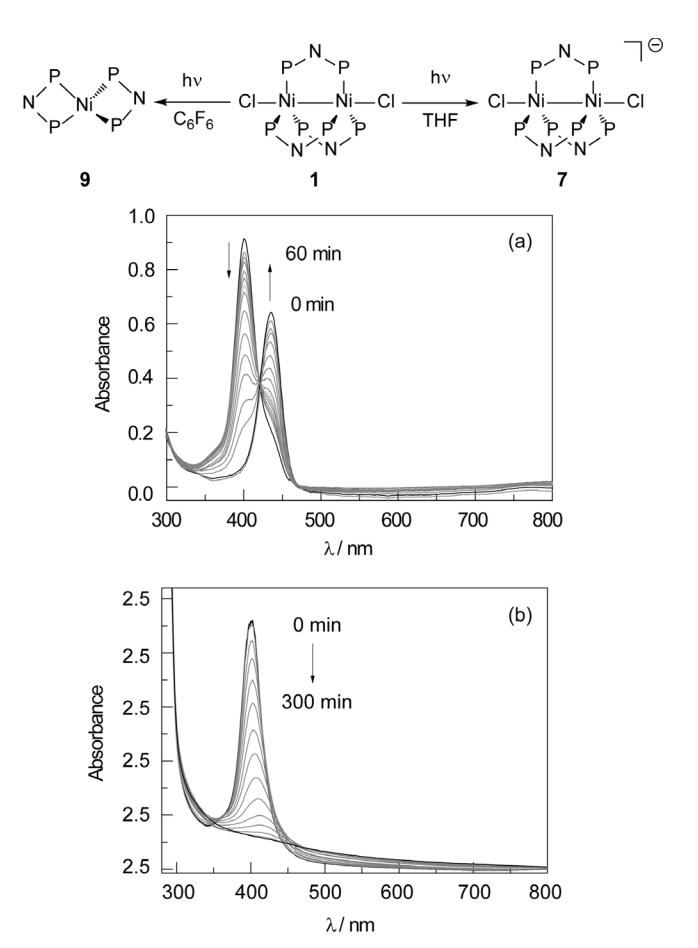


Figure 5. Spectral evolution during photolysis ($\lambda > 320$ nm) of Ni₂[I,I]Cl₂ complex 1 (a) in THF and (b) in C₆F₆.

400 nm range consist of mixed MMCT and metal-to-ligand charge transfer (MLCT), with the ligand character largely consisting of low-lying unoccupied phosphine p character (Figure S35). A chloride-based $Cl(p_z) \rightarrow Ni(d_{z^2})$ LMCT transition is found at ~270 nm, and thus is predicted to coincide with the higher energy absorption band(s) with energies > 300 nm (Table S16). This LMCT transition red shifts to ~300 nm in the bromide analogue 4 (Table S17).

Steady-state photolysis with a 1000 W Hg/Xe lamp ($\lambda > 320$ nm) of Ni₂[I,I] complex 1 in solvent containing weak C–H bonds, such as THF (C–H BDE⁴² = 92 kcal mol⁻¹), leads to the generation of a light green-colored solution over the course of the photoreaction (Figure 5a). Comparison of the *in situ* UV-vis (Figure S32) and EPR (Figure S17) spectra obtained from steady-state photolysis of complex 1 in THF with a spectra from an independently prepared sample of the complex 7 confirmed the identity of the photoproduct as the one electron reduced anionic Ni₂[I,0]Cl₂ complex.

When the photolysis ($\lambda > 320$ nm) is run in hexafluorobenzene, the green solution becomes colorless (Figure 5b). The identity of the colorless photoproduct was established to be Ni(tfepma)₂ (**9**) by comparison with an independent sample prepared by treatment of Ni(0) with 2 equivalents of tfepma. 1 H, $\{^1$ H $\}^{31}$ P NMR, and electronic spectroscopy were used to characterize complex **9**, and X-ray crystallographic analysis of a single crystal established **9** to be a pseudotetrahedral Ni(0) with the structure shown in Figure S25. The photogenerated Cl radicals are expected to evolve Cl₂ gas, as H

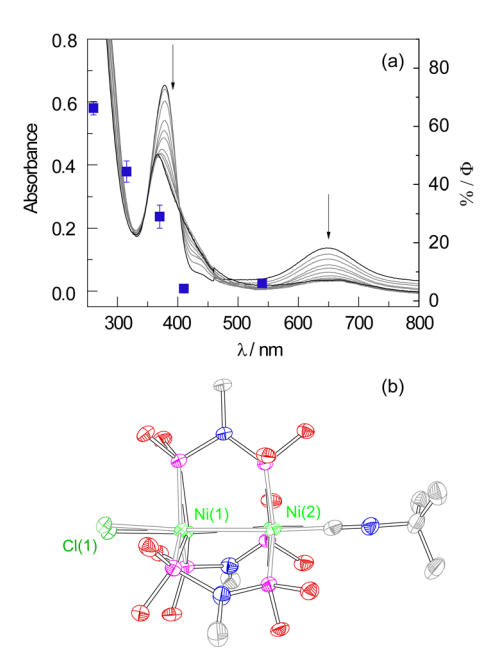


Figure 6. (a) Steady-state photolysis of complex 3 (λ > 320 nm) in THF and photochemical quantum yields (Φ) as a function of excitation wavelength. (b) Thermal ellipsoid plots of photogenerated structure (solid) superimposed on the dark structure of complex 3 (faded). The H atoms and $-CH_2CF_3$

atom abstraction is hampered in the absence of C–H bonds in the solvent. We proposed that excitation of the $d\sigma \to d\sigma^*$ transition results in photoactivation of the Ni–X bond to expel Cl• along with the formation of the tfepma-bridged $d^{10}\text{-}d^{10}$ binuclear Ni₂[0,0] species, which ultimately decomposes to the 4-coordinate Ni complex 9.

Photolysis of a THF solution of **3** (λ > 320 nm) resulted in the consumption of **3** and clean formation of **6** (Figure 6a). The photochemical action spectrum was constructed by measuring wavelength-dependent (260, 315, 370, 410, 540 nm) quantum yield measurements (Φ) for halogen elimination from **3** in THF against a potassium ferrioxalate standard actinometer (Figure 6a). ^{43,44} These data indicate that the highest quantum yields correlate with the high energy LMCT band (~270 nm).

Trap-free solid-state halogen photoelimination reactions have been previously observed in mono- and binuclear complexes of $Pt(III)^{6,10}$ and $Au(III)^7$ as well as in mononuclear Ni(III) complexes. ^{20,21} Solid-state photolysis from binuclear Ni complexes were pursued, motivated by the steady-state photolysis results of complex 1 in C_6F_6 and the high quantum yields of complex 3 in solution. Irradiation (~20 Torr, 20 °C, λ > 305 nm) of complexes 1 and 3 in the solid-state for 18 h results in the formation of compounds 8 and 6, respectively, along with the evolution of Cl_2 gas. The evolved Cl_2 was treated with N_1N_1 -diethyl-1,4-phenylene-diamine sulfate (DPD) and the resulting DPD⁺⁺Cl⁻⁻ was analyzed colorimetrically to reveal 80 and 72% yields of Cl_2 from 1 and 3, respectively (Figure S33).

Building upon our previous photocrystallography experiments to identify photoelimination intermediates, 11,20, 45 steady-state photocrystallography techniques were used to probe the photoinduced structural changes in complex 3 that promote the halogen elimination chemistry. Diffraction data collected prior to

and during irradiation ($\lambda_{\rm exc}=300$ nm, 20 K) generated a photodifference map, showing the presence of a photoinduced structure populated at 10.6% of the overall crystal (Figure S27). The photodifference map demonstrates that the Ni–Cl bond distance elongates from 2.4127(9) to 2.495(3) Å, while the Ni–Ni bond significantly contracts from 2.9264(6) to 2.600(2) Å, which is the bond length for the ground state of complex **6** (Figure 6b). The excited state is therefore a mixture of Cl• and photoproduct **6**. Variable-temperature crystallography of single crystals of **3** revealed that the metrical parameters do not significantly vary with temperature, confirming that the observed structural changes are not caused by a thermal process over the temperature range of 20-300 K (Figure S28 and Table S8).

3. Conclusions

In summary, low-valent binuclear d^9-d^9 and d^9-d^{10} Ni complexes have been prepared that are capable of Ni–X bond photoactivations with the expulsion of halogen radicals by excitation into a $d\sigma^*$ transition that has significant LMCT character. Utilization of metalmetal bonds in the three-fold symmetry provides a new design strategy to achieve halogen photoelimination from low-valent binuclear Ni centers. Experimental and computational studies establish an electronic structure that is dominated by $d\sigma^*$ character with a significant halide admixture that engenders anti-bonding character with respect to M–X bonds. It stands that future tuning of the electronic structure of the ligand scaffold could yield a catalyst that will also be able to reduce HCl to the constituent H_2 , allowing for the HX-splitting photocycle to be closed.

vCRediT authorship contribution statement

SJH, SR, DG: compound preparation, photochemistry, compound characterization, spectroscopy and X-ray structural characterization. RGH: computational chemistry. SLZ: X-ray crystallography. YSC: photocrystallography. DGN and all other authors: design and interpretation of experiments, manuscript preparation.

Declaration of Competing Interest

The authors declare that they have no known competing financial interests or personal relationships that could have appeared to influence the work reported in this paper.

Appendix A. Supplementary data

CCDC 1573297, 1573296, 1573295, 1573294, 1573292, 1573291 and 1573293 contains the supplementary crystallographic data for **1**, **3**, **5**, **6**, **7**, **8** and **9**, respectively. These data can be obtained free of charge via http://www.ccdc.cam.ac.uk/conts/retrieving.html, or from the Cambridge Crystallographic Data Centre, 12 Union Road, Cambridge CB2 1EZ, UK; fax: (+44) 1223-336-033; or e-mail: deposit@ccdc.cam.ac.uk. Detailed experimental procedures, compound preparation and characterization, spectroscopic data, crystallographic data, computational results, XYZ coordinates of computed spectra and structures.

Acknowledgements

This work was supported by the National Science Foundation under grant CHE-1855531. RGH acknowledges support from the ANL Enrico Fermi Fellowship. DG acknowledges the National Science Foundation (NSF) for a Graduate Research Fellowship Program (GRFP). We thank James Lawniczak for help with ligand preparations. Photocrystallography was carried out at ChemMatCARS, Sector 15, APS, which is principally supported by the Divisions of Chemistry (CHE) and Materials Research (DMR), National Science Foundation, under grant number NSF/CHE-1346572. Use of the PILATUS3 X CdTe 1M detector is supported by the National Science Foundation under the grant number NSF/DMR-1531283. Use of the Advanced Photon Source, an Office of Science User Facility operated for the U.S. Department of

References

- (1) N.S. Lewis, D.G. Nocera, Proc. Natl. Acad. Sci. U.S.A. 103 (2006) 15729.
- (2) T.R. Cook, D.K. Dogutan, S.Y. Reece, Y. Surendranath, T.S. Teets, D.G. Nocera, Chem. Rev. 110 (2010) 6474.
- (3) D.G. Nocera, Inorg. Chem. 48 (2009) 10001.
- (4) A. J. Esswein, D. G. Nocera, Chem. Rev. 107 (2007) 4022.
- (5) A. F. Heyduk, D.G. Nocera, Science 293 (2001) 1639.
- (6) T. R. Cook, Y. Surendranath, D.G. Nocera, J. Am. Soc. Chem. **131** (2009)
- (7) T. S. Teets, D.G. Nocera, J. Am. Chem. Soc. 131 (2009) 7411.
- (8) D.C. Power, M.B. Chambers, T.S. Teets, N. Elgrishi, B.L. Anderson, D.G. Nocera, Chem. Sci. 4 (2013) 2880.
- (9) A.R. Karikachery, H.B. Lee, M. Masjedi, A. Ross, M.A.; Moody, X. Cai, M. Chui, C.D.; Hoff, P.R. Sharp, Inorg. Chem. 52 (2013) 4113.
- (10) H. Yang, F.P. Gabbaï, J. Am. Chem. Soc. 136 (2014) 10866.
- (11) D.C. Powers, S.J. Hwang, B.L. Anderson, H. Yang, S.L. Zheng, Y.S. Chen, T.R. Cook, F.P. Gabbaï, D.G. Nocera, Inorg. Chem. 55 (2016) 11815.
- (12) S. Sahu, F.P. Gabbaï, J. Am. Chem. Soc. 139 (2017) 5035.
- (13) E.I. Carrera, T.M. McCormick, M.J. Kapp, A.J. Lough, D.S. Seferos, Inorg. Chem. 52 (2013) 13779.
- (14) H. Yang, F.P. Gabbaï, J. Am. Chem. Soc. 136 (2014) 10866.
- (15) T.P. Lin, F.P. Gabbaï, J. Am. Chem. Soc., 134 (2012) 12230.
- (16) E.I. Carrera, D.S. Seferos, Dalton Trans. 44 (2015) 2092.
- (17) E.I. Carrera, A.E. Lanterna, A.J. Lough, J.C. Scaiano, D.S. Seferos, J. Am Chem. Soc. 138 (2016) 2678.
- (18) C.M. Lemon, S.J. A.G. Maher, D.C. Powers, D.G. Nocera, Inorg. Chem. 57 (2018) 5333.
- (19) C.H. Lee, D.A. Lutterman, D.G. Nocera, Dalton Trans. 42 (2013) 2355.
- (20) S.J. Hwang, D.C. Powers, A.G. Maher, B.L. Anderson, R.G. Hadt, S.L. Zheng, Y.S. Chen, D.G. Nocera, J. Am. Soc. Chem. 137 (2015) 6472.
- (21) S.J. Hwang, B.L. Anderson, D.C. Powers, A.G. Maher, R.G. Hadt, D.G. Nocera, Organometallics 34 (2015) 4766.
- (22) R. Fayad, S. Engl, E.O. Danilov, C.E. Hauke, O. Reiser, F.N. Castellano, J. Phys. Chem. Lett. 11 (2020) 5345.
- (23) J.K. McCusker, Acc. Chem. Res. 36 (2003) 876.
- (24) E.A. Juban, A.L. Smeigh, J.E. Monat J.K. McCusker, Coord. Chem. Rev. 250 (2006) 1783.
- (25) T.T. Tsou, J.K. Kochi, J. Am. Chem. Soc. 101 (1979) 7547.
- (26) J.M. Coronas, G. Muller, M. Rocamora, J. Organomet. Chem. **301** (1986)
- (27) R.M. Ceder, J. Granell, G. Muller, M. Font-Bardía, X. Solans, Organometallics 15 (1986) 4618.

Energy (DOE) Office of Science by Argonne National Laboratory, was supported by the U.S. DOE under Contract No. DE-AC02-06CH11357. We gratefully acknowledge the computing resources provided on Blues, a high-performance computing cluster operated by the Laboratory Computing Resource Center at Argonne National Laboratory (ANL). We present this work in recognition of the accomplishments and penetrating contributions by Professor Malcolm Green to our understanding of organometallic chemistry and synthetic materials science.

- (28) P.T. Matsunaga, G.L. Hillhouse, A.L. Rheingold, J. Am. Chem. Soc. 115 (1993) 2075.
- (29) K. Koo, G.L. Hillhouse, Organometallics 14 (1995) 4421.
- (30) A.T. Higgs, P. J. Zinn, S. J. Simmons, M.S. Sanford, Organometallics 28 (2009) 6142.
- (31) D.C. Powers, B.L.; Anderson, D.G. Nocera, J. Am. Chem. Soc. 135 (2013) 18876.
- (32) S. J. Hwang, D.C. Powers, A.G. Maher, D.G. Nocera, Chem. Sci. 6 (2015)
- (33) C.H. Lee, T.R. Cook, D.G. Nocera, Inorg. Chem. 50 (2011) 714.
- (34) S.J. Tereniak, E.E. Marlier, C.C. Lu, Dalton Trans. 41 (2012) 7862.
- (35) A. J. Esswein, A.S. Veige, D.G. Nocera, J. Am. Chem. Soc. 127 (2005) 16641.
- (36) T.R. Cook, A.J. Esswein, D.G. Nocera, J. Am. Chem. Soc. 129 (2007) 10094.
- (37) T.S. Teets, D.A. Lutterman, D.G. Nocera, Inorg. Chem. 49 (2010) 3035.
- (38) B.R. Dibble, M.S. Sigman, A.M. Arif, Inorg. Chem. 44 (2005) 3774.
- (39) C.Y.; Lin, P.P. Power, Chem. Soc. Rev. 46 (2017) 5347.
- (40) D.L. DeLaet, R.d. Rosario, P.E. Fanwick, C.P. Kubiak, J. Am. Chem. Soc. 109 (1987) 754.
- (41) G.M. Ferrence, E. Simón-Manso, B.K. Breedlove, L. Meeuwenberg, C.P. Kubiak, Inorg. Chem. 43 (2004) 1071.
- (42) L.J.J. Laarhoven, P. Mulder, D.D.M. Wayner, Acc. Chem. Res. **32** (1999)
- (43) J.N. Demas W.D. Bowman E.F. Zalewski, R.A. Velapoldi, J. Phys. Chem. 85 (1981) 2766.
- (44) H. Kuhn, S.E. Braslavasky, R. Schmidt, Pure Appl. Chem. 76 (2004) 2105.
- (45) D.C. Powers, B.L. Anderson, S.J. Hwang, T.M. Powers, L.M. Pérez, M.B. Hall, S.L. Zheng, Y.S. Chen, D.G. Nocera, J. Am. Chem. Soc. 136 (2014) 15346